ACS Catalysis

Research Article

pubs.acs.org/acscatalysis

Operando and Kinetic Study of Low-Temperature, Lean-Burn Methane Combustion over a Pd/γ-Al_2O_3 Catalyst

Jing Xu,[†] Like Ouyang,[†] Wei Mao,[†] Xue-Jing Yang,[†] Xin-Chao Xu,[†] Jun-Jie Su,[†] Ting-Zhou Zhuang,[†] Hui Li,[‡] and Yi-Fan Han*[,†]

[†]State Key Laboratory of Chemical Engineering, East China University of Science and Technology, Shanghai, 200237, People's Republic of China

[‡]Department of Chemistry, Shanghai Normal University, Shanghai, 200234, People's Republic of China

ABSTRACT: Operando and kinetic studies of lean-burn methane combustion were preformed on a Pd(3.3 wt %)/γ-Al_2O_3 catalyst in a low temperature range of 473−673 K. The reaction order with respect to oxygen decreased with temperature, and the order with respect to methane remained constant. The working catalyst is characterized using operando Raman spectroscopy and in situ diffuse reflectance infrared Fourier transform spectroscopy of CO adsorption (DRIFTS), and the Pd chemical states were measured with X-ray photoelectron spectroscopy (XPS). Partial oxidation of Pd atoms during reaction was identified by Raman and XPS spectroscopies. In particular, the DRIFT spectra revealed that ∼45% of Pd atoms at the top layers were transferred into PdO_x species above 523 K. The reaction was assumed to occur primarily on the metallic Pd sites below 673 K, proceeding through the Langmuir−Hinshelwood mechanism, and Pd oxide may affect the adsorption and activation of reactants.

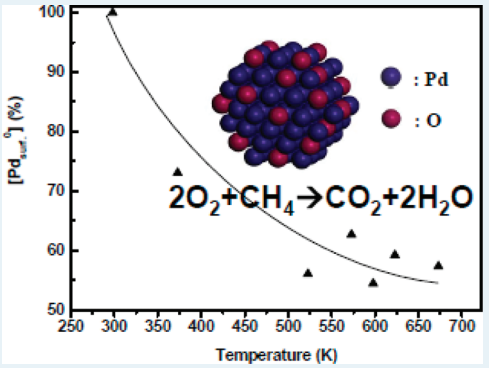

KEYWORDS: *kinetics, low-temperature methane combustion, operando spectroscopy, Raman, in situ DRIFTS, Pd/γ-Al_2O_3, catalyst*

1. INTRODUCTION

Methane, as an attractive, clean fuel, gives off lower levels of pollutants, such as NO, CO_x, and other toxic gases, than solid fossil fuels during combustion.[1−5] Recently, however, more strict safety recommendations have enforced a limit level of explosive exhaust gases for methane emissions from coal mines and other gas reserve sites. The potential contribution of methane to the global greenhouse effect has proven to be about 20 times stronger than carbon dioxide.[3] The concentration of methane in air has been increasing at a rate of 1%/year during the past decade, and the growth rate is faster than that for CO_2.[3]

For economic and environmental concerns, incineration is still an effective way to remedy methane released from industry; however, this process is infeasible economically when treating dilute methane (<0.5%), or to say, the lean-burn methane combustion, because continuous fueling is required during thermal combustion at above 1273 K. In the case of ventilation air methane (VAM) from coal mines, catalytic combustion (<1000 K) of 1% methane by lean-burn turbines to generate electricity using catalytic reactors is believed to be a feasible and relatively cost-effective option for recycling that energy.[6] Lowering the temperature of ignition can reduce the preburner zone, muffle the emission of air pollutants, and improve the fuel efficiency in gas turbines.[7,8] Currently, one of the key issues of methane combustion is to develop highly active catalysts that can enhance the combustion of dilute methane at low temperatures. Therefore, mechanistic insight into this reaction is paramount for the rational design of high-efficiency combustion catalysts.

Methane combustion on the real and model Pd catalysts has long been studied.[9−11] Despite contradictory mechanisms that have been proposed, a common point is that the layer or bulk Pd oxide (PdO_x) produced by oxidizing metallic Pd during reactions may work as active sites at or below 1055 K;[12] above this temperature, the reaction occurs mainly on the metallic Pd atoms resulting from the decomposition of PdO_x. During reaction, CH_x species produced from the dissociation of methane likely react with the lattice oxygen of PdO_x following a Mars−van-Krevelen mechanism, and the activation of the first C−H bond of the methane molecule has proven to be the rate-determining step.[13−19] On the other hand, an alternative Langmuir−Hinshelwood mechanism has also been proposed, wherein methane was fully oxidized through interactions between CH_x species and oxygen on Pd surfaces.[20,21] However, most of experimental evidence for mechanistic studies was achieved above 673 K, which was regarded as the takeoff point of this reaction. To date, fundamental aspects concerning reaction behavior and the origin of active sites on supported Pd catalysts in the low-temperature region, especially lower than 673 K, have rarely been addressed,[22] except for an earlier preliminary kinetic study at 550 K reported by Ribeiro et al.[15,23] Part of the reason is that the precious metal catalysts usually exhibit very poor activity toward this reaction at relatively low temperatures.[9]

Received: October 27, 2011
Published: January 2, 2012

Methane combustion on Pd catalysts has proven to be affected by several factors, such as the partial pressure of the reactants, reaction temperatures, catalyst properties, and so forth.[3,9] It is known that metallic Pd atoms are easily oxidized to form PdO_x species on the Pd surface, even at room temperature under reaction conditions. PdO_x was suggested to significantly change the catalytic properties through altering the bond strength of the Pd adsorbate. However, the method of quantitative determination of PdO_x and its role in methane combustion at low temperatures are still limited. In the present study, to investigate the low-temperature reaction behavior, the kinetics of the lean-burn methane combustion on a Pd/γ-Al_2O_3 catalyst was measured in the temperature range 473−673 K. With the improvement of instrumental accuracy, we also determined the kinetics at or above 673 K, as well, even though it was reported several decades ago.

In the meantime, the undergoing structural changes in the catalyst surface during reaction were studied by real time in situ/operando spectroscopic methods, such as laser Raman spectroscopy (LRS) and diffuse reflectance infrared Fourier transform spectroscopy (DRIFTS) using CO as the probe molecule. The change in electronic structure was characterized with X-ray photoelectron spectroscopy (XPS). The operando Raman scattering technique, as a cutting-edge and powerful tool, was also used for probing molecular vibrations occurring at low wavenumbers, where metal oxides exhibit characteristic lines. The Raman spectrum can be recorded under realistic reaction conditions with simultaneous real-time online analysis of reaction products. In particular, this technique has proven to be sensitive even to minor changes of the Pd surface owing to thermal or reaction induction.[4,5,19,22,24−31] We believe in situ/operando spectroscopies in combination with kinetics is a convenient and versatile technique for the investigation of the relationship of the catalyst structure and activity.

2. EXPERIMENTAL SECTION

2.1. Catalyst Preparation and Reactivity Measurements. Palladium was introduced into the system as Pd (3.3 wt %) supported on a γ-Al_2O_3 powder (200 mesh) having a BET surface area of ∼237 $m^2 \cdot g^{-1}$. The catalyst was prepared by incipient wetness impregnation using an aqueous solution of $Pd(NO_3)_2$. The obtained precursors were dried in an oven at 393 K overnight.

Kinetic measurements were carried out using a microplug-flow reactor in a stream of CH_4 (0.1−1.0 kPa), O_2 (3.0−10.0 kPa) and He (balance gas) with varying gas hourly space velocities (GHSV) from 6,000 to 36,000 h^{-1} at atmospheric pressure. Prior to experiment, the catalyst was pretreated at 673 K in O_2 and then reduced in H_2 with a flow rate of 20 mL/min for 30 min each time. In order to obtain differential reaction rates, methane conversion was controlled below 10% by diluting the catalyst with α-Al_2O_3 powders in ratios ranging from 1 to 1000. Analysis was performed with an online gas chromatograph (Shimadzu GC-2010) equipped with a CP-carbonBOND column. Each data point was taken at an interval of 2 h. Absolute mass-specific reaction rates and turnover rates were calculated from the average concentrations of each component $\dot{c}_i$, at the inlet and outlet of the reactor:

$$r_{CH_4} = \frac{\dot{c}_{CH_4,in} \cdot X_{CH_4} \cdot \dot{V}_{gas}}{m_{Pd}} [mmol \cdot min^{-1} \cdot g_{Pd}{}^{-1}] \quad (1)$$

where m_{Pd}: mass of Pd in the reactor bed, $\dot{V}$: total molar flow rate, X_{CH_4}: conversion of methane based on CO_2 formation, $\dot{c}_{CH_4}$: concentration of methane in gas mixture, equal to p_i/p_0, p_i: partial pressure of reactants, p_0: total pressure in the system.

Sequentially, the reaction rate for methane combustion expressed in the turnover frequency (r_{TOF}, s^{-1}) was obtained by eq 2

$$r_{TOF} = \frac{r_{CH_4} \cdot M_{Pd}}{D_{Pd}} [s^{-1}] \quad (2)$$

where M_{Pd}: atomic weight of Pd, D_{Pd}: dispersion of Pd atoms exposure to reactants evaluated on the basis of the model of semihemispheric ball, about 20% dispersion of Pd was calculated according to an average size of 8.0 nm for Pd particles, which was measured by transmission electron microscopy (TEM, Tecnai TF 20 S-twin with Lorentz Lens).

In addition, the reaction potentially inhibited by the products was carefully determined by dosing excess amount of CO_2 (0.1 kPa) and H_2O (0.2 kPa) (passing by water vapor at controlled temperature). On the other hand, for the determination of the rate affected by heat or mass transport limitations, a Pd (0.6 wt.%, d_{Pd}: 7.8 nm) was also prepared following the same method and tested for the Koros-Nowak experiment.[23,32] This catalyst also exhibited relatively high stability with losing only about 5% activity after reaction (0.5 kPa CH_4, 3.0 kPa O_2, 0.2 kPa H_2O, in He) 10 h at 673 K with a GHSV of 36000 h^{-1}.

2.2. Characterization. *2.2.1. LRS.* Raman spectra were measured with an in situ setup using a Raman microscope (LabRAM HR, Horiba JY) equipped with a thermoelectrically cooled CCD array detector and a high grade Leica microscope (long working distance objective 50 ×). The sample was placed into a sample cell, specially designed for catalytic reactions at high temperature and pressure (CCR1000, Linkam fitted with quartz windows). The sample was mounted on an unreactive disposable ceramic fabric filter placed inside a ceramic heating element, which was capable of heating samples from ambient up to 1273 K. The reaction conditions were the same as those for the microfixed bed reactor. The gases were introduced into the catalyst stage via a 1/16 in. gas line, and passed through the sample and ceramic fabric filter at a flow rate of ∼50 mL/min. The flow rates of the reactant gases were controlled by mass flow controllers. Raman measurements were performed on a sample spot irradiated by a visible 514.5 nm argon ion laser. The laser power from the source was around 25 mW. Heating induced by the laser, which usually interferes with the acquiring of the real spectroscopy, was controlled carefully. Thus, the laser power was minimized as much as possible by lowering the power using density filter and optimizing the time for scanning without sacrificing too much on the Raman signals. It is estimated that only about 1−2 mW of the laser power reached the samples during the measurements, so the in situ Raman signals are noisy, and high precision of the peaks at corresponding wave numbers was not available. The scanning time for each Raman spectrum was ∼360 s, with a spectral resolution around 1−1.3 cm^{-1}. The temperature ramping rate was 10 K/min when the sample was heated from 298 to 673 K. The products were analyzed with an online mass spectroscopy (HPR-20, Hiden Analytical Ltd.).

2.2.2. DRIFTS. CO adsorption on the Pd/γ-Al_2O_3 catalyst was conducted in a reaction cell (modified Harricks model HV-DR2) to allow gas flowing continuously through the catalyst bed (∼0.02 g) during spectra acquisition. The spectra were

dx.doi.org/10.1021/cs200694k | ACS Catal. 2012, 2, 261−269

recorded on a PerkinElmer FT-IR spectrum 100 (resolution: 4 cm^{-1}) spectrometer with a liquid-nitrogen-cooled mercury cadmium telluride (MCT) detector. Contributions from gas phase CO were eliminated by subtracting the corresponding spectra from the pure KBr powder.

Ahead of CO adsorption, the catalyst was first pretreated following the same procedure as described in section 2.1, and then the reaction was carried out at different temperatures using the same feed gas (3.0 kPa O_2 and 0.5 kPa CH_4 in He, 50 mL/min) for 2 h. The system was either cooled down to 298 K in He (20 mL/min) or remained following a purge (5 min) with He. Finally, a gas mixture of 1.0 kPa CO in He (20 mL/min, 30 min) was used for adsorbing CO. To avoid the potential reduction of Pd oxide caused by adsorbed CO, all spectra were recorded within 10 min.

To calculate the concentration of the metallic Pd atoms on the catalyst surface, a straight line connecting the first and last peaks was chosen as the baseline.

2.2.3. XPS. XPS analysis was performed on a VG Escalab 250 spectrometer, using Al−K_α radiation (1486.6 eV, pass energy 20.0 eV). The base pressure of the instrument is 1×10^{-9} Torr. The background contribution B (E) (obtained by the Shirley method) caused by an inelastic process was subtracted, and the curve-fitting was performed with a Gaussian−Lorentzian profile by a standard software. The binding energies (BEs) over supported catalysts were calibrated using the C1s peak at 285.0 eV. The instrument was also calibrated by using Au wire. XPS spectra were recorded at $\theta = 90°$ of X-ray sources.

3. RESULTS AND DISCUSSION

3.1. Determination of Kinetics Measurements Potentially Affected by Several Factors. *Effects of CO_2 and H_2O.* The inhibition of products on methane combustion in a similar reaction system has been reported by Ribeiro et al.[15,23] It was found that the reaction rate at 553 K for a Pd (0.86 wt %)/ZrO_2 catalyst could be decreased by one magnitude with increasing the H_2O concentration from ~0 to 1.0% but remained unchanged when CO_2 concentration was <3.5%. In this study, the kinetic measurements were carried out by controlling the methane conversion below 10%. It means that the maximum concentration of CO_2 and H_2O in the reaction system should be ~0.1% and 0.2%, respectively, during kinetic measurements. In the case of CH_4 (0.5 kPa), O_2 (3.0 kPa), and rest He, a typical composition of feed gas in kinetic measurements may produce 0.05% CO_2 and 0.1% H_2O with a methane conversion of 10%. Table 1 indicated that the rate was not affected from

Table 1. Effects of CO_2 and H_2O on Methane Combustion at Different Temperatures, Rates in TOF (s^{-1})[a]

feed gas	473 (K)	573 (K)	673 (K)
no additional CO_2 and H_2O	0.13	2.82	67.21
dose CO_2 (0.1 kPa)	0.13	2.80	68.10
dose H_2O (0.2 kPa)	0.11	2.58	64.92

[a]The reaction was carried out in a feed gas of 0.5 kPa CH_4, 3.0 kPa O_2, in He while adding CO_2 and H_2O; GHSV: 36 000 h^{-1}. The conversion of methane was maintained under 10% by diluting with α-Al_2O_3 powders.

dosing of 0.1 kPa CO_2 and mildly dropped by 15.0% (473 K), 7.8% (573 K), and 4.6% (673 K) as a result of dosing 0.1 kPa H_2O. To obtain the differential rate, 0.2 kPa H_2O was added into the system if without a specific statement. It is noted that the further increase in CO_2 and H_2O concentration may remarkably change the reaction rate by poisoning the active sites;[23] however, those experiments are beyond the scope of this study.

Heat and Mass Transfer Limitations. Because methane combustion is a highly exothermic reaction, a Koros−Nowak test was performed at 573 K on catalysts with different Pd loading amounts. As listed in Table 2, by decreasing the Pd loading amount to 0.6 wt %, the rate in TOF remained almost unchanged under the same reaction conditions, demonstrating that there were no heat and mass transfer limitations in our system.

Table 2. Test for Heat and Mass Transfer Limitations[a]

catalyst	rate in TOF (s^{-1})	Pd particle size (d: nm)	dispersion of Pd atoms (%)
Pd (3.3 wt %)/γ-Al_2O_3	2.58	8.0	20
Pd (0.6 wt %)/γ-Al_2O_3	2.64	7.8	22

[a]The reaction was carried out at 573 K in a feed gas of 0.5 kPa CH_4, 3.0 kPa O_2, 0.2 kPa H_2O, in He while adding CO_2 and H_2O; GHSV: 36 000 h^{-1}. The conversion of methane was maintained under 10% by diluting with α-Al_2O_3 powders.

3.2. Kinetics. Figure 1a shows the pressure-dependent reaction rates on the partial pressure of oxygen (p_{O_2}), ranging

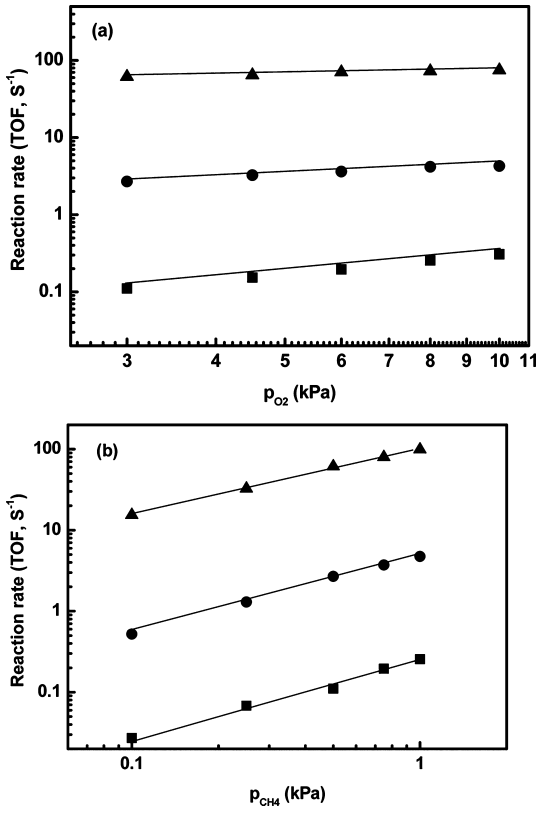

Figure 1. Dependence of reaction rates on the partial pressure of reactants at 473 (■), 573 (●), 673 K (▲). (a) 3.0−10.0 kPa O_2, 0.5 kPa CH_4, 0.2 kPa H_2O, in He; (b) 0.1−1.0 kPa CH_4, 3.0 kPa O_2, 0.2 kPa H_2O, in He. Dilute ratios with α-Al_2O_3 powders: pure to 1/1000, GHSV: 6000−36 000 h^{-1}.

dx.doi.org/10.1021/cs200694k | ACS Catal. 2012, 2, 261−269

from 3.0 to 10.0 kPa while keeping the partial pressure of methane (p_{CH_4}) at 0.5 kPa. The reaction rates increased with an increase in p_{O_2}, yielding orders of 0.86, 0.38, and 0.16 with respect to oxygen (α) at 473, 573, and 673 K. On the other hand, by keeping p_{O_2} at 3.0 kPa while increasing p_{CH_4} from 0.1 to 1.0 kPa (Figure 1b), the orders with respect to methane (β) were 0.95, 0.97, and 0.81 at 473, 573, and 673 K. The reaction rates increased with temperature by varying p_{CH_4} from 0.1 to 1.0 kPa while keeping p_{O_2} at 3.0 kPa (Figure 2). The Arrhenius

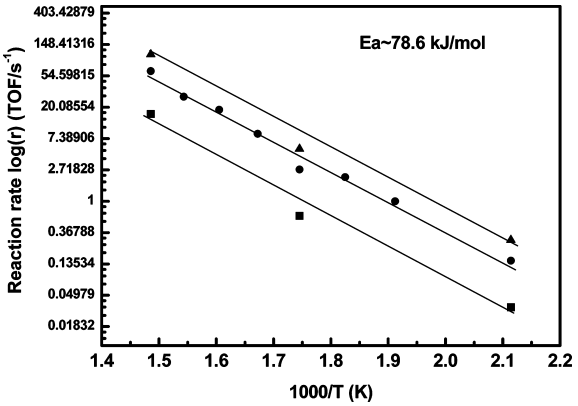

Figure 2. Arrhenius plots of the reaction rate ($\log(r)$) vs $1/T$ for methane combustion at 0.1 (■), 0.5 (●), 1.0 kPa (▲) CH_4, respectively while keeping 3.0 kPa O_2, 0.2 kPa H_2O in He. Dilute ratio with α-Al_2O_3 powders: pure to 1/1000, GHSV: 6000−36 000 h^{-1}.

plots of the reaction rates at different p_{CH_4}/p_{O_2} ratios yield an apparent activation energy (E_a) of 78.6 ± 5.0 kJ/mol.

Kinetic data obtained for several typical alumina supported Pd catalysts and a Pd wire under similar reaction conditions are summarized in Table 3. The rates in TOF in the temperature range 473−573 K are close to the data obtained from various Pd/Al_2O_3 and unsupported pure Pd catalysts. A common feature derived from those data is positive reaction orders for methane (0.6−1.0) and near zero-order for oxygen (except 0.1 for the Pd wire[7] and Pd single crystals[47]). In addition, the orders for methane conversion at different temperatures are very close to the literature data; however, a significant drop in the orders for oxygen from 0.86 at 473 K to 0.16 at 673 K was observed, indicating the variation of the reaction behavior. The E_a values and the rates in turnover frequency (TOF) for all catalysts below 673 K are rather comparable. In contrast, the reported E_a values above 673 K were distributed in a broad range, probably because the reaction was strongly affected by factors such as reaction conditions, morphology, Pd oxide states, and the size of the Pd particles,[9] but further discussion of such an issue is beyond the scope of this study. Interestingly, Cullis et al.[33] also found a drastic drop of E_a from 84 (<680 K) to 23 kJ/mol (>680 K) on a Pd (2.7 wt %)/γ-Al_2O_3 catalyst; unfortunately, this phenomenon has not yet been explained.

3.2. Characterization. Figure 3 shows XPS Pd3d spectra recorded from the fresh and spent catalysts. The BE of $Pd3d_{5/2}$ was 335.4 eV for the fresh catalyst and varied in a range from 336.0 to 336.7 eV after reaction at different temperatures, an indication of a transformation from Pd to PdO_x.[34,35] However, by those data it is still difficult to estimate the ratio of Pd/Pd^{2+} on the working catalyst surfaces because the surface reconstruction and the depositing of contaminants during reaction

Table 3. Comparisons of Kinetics Data for Methane Combustion over Pd/γ-Al_2O_3 Catalysts; Power Law Functionality:[a] $\gamma_{CH_4} = k(p_{O_2}/p_{total})^{\alpha}(p_{CH_4}/p_{total})^{\beta}$

catalysts	experimental method	reactant mixture	E_a[a] (kJ/mol)	rate (γ_{CH_4}, TOF/s^{-1})	α		β		ref
Pd (2.7 wt %)/γ-Al_2O_3	pulse flow microreactor	CH_4/O_2 = 1:10−10:1	84 ± 3 (<680 K); 23 ± 2 (>680 K)	2.28	(623 K)	0	1.0	(623 K)	33
Pd (0.04 wt %)/γ-Al_2O_3	continuous flow microreactor	CH_4/O_2 = 1:10	71.1 (523−573 K); 83.6 (623−773 K)	0.31	(573 K)	0	0.6	(573 K)	7
Pd (1.0−10.0 wt %)/γ-Al_2O_3	continuous flow microreactor	CH_4/O_2 = 1:22	76	N.A.[b]		0	1	(550 K)	23
Pd wire		CH_4/O_2 = 1:4	71.0	5.4	(773 K)	0.1	0.8	(773 K)	7
Pd(111)	UHV chamber	CH_4/O_2 = 1:10	140 ± 20	2.8−2.9	(598 K)	−0.1	0.8	(598 K)	47
Pd(100)	UHV chamber	CH_4/O_2 = 1:10	125 ± 15	5.0−5.3	(598 K)	0.1	0.8	(598 K)	47
Pd(110)	UHV chamber	CH_4/O_2 = 1:10	160 ± 20	1.2−1.4	(598 K)	0.2	0.7	(598 K)	47
Pd (3.3 wt %)/γ-Al_2O_3	continuous flow microreactor	CH_4/O_2 = 1:3−30	78.6 ± 5.0	0.03−0.29	(473 K)	0.86	0.95	(473 K)	this study
				0.53−4.47	(573 K)	0.38	0.97	(573 K)	
				15.0−99.8	(673 K)	0.16	0.81	(673 K)	

[a] E_a was measured in the temperature range 473−673 K; reaction rates (partial pressure of reactants was given in column 3). [b] N.A.: not available.

dx.doi.org/10.1021/cs200694k | ACS Catal. 2012, 2, 261−269

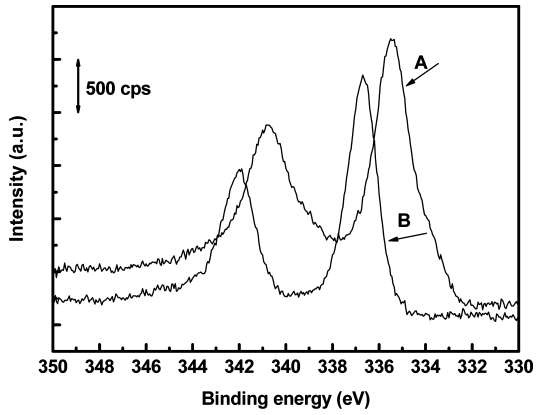

Figure 3. XPS spectra of Pd3d (A, fresh; B, spent). The reaction was carried out in a stream of 0.5 kPa CH_4, 3.0 kPa O_2 in He; GHSV: 36 000 h^{-1} at 673 K for 2 h.

may give rise to a large uncertainty of the XPS results. In situ/operando spectroscopy may help to circumvent these problems.

Operando Raman spectra in Figure 4 show the structural modifications of Pd particles at different temperatures. For comparison, the spectra were first recorded in O_2 (3.0 kPa O_2 in He, Figure 4a). Almost no peak appeared at 298 K, and three

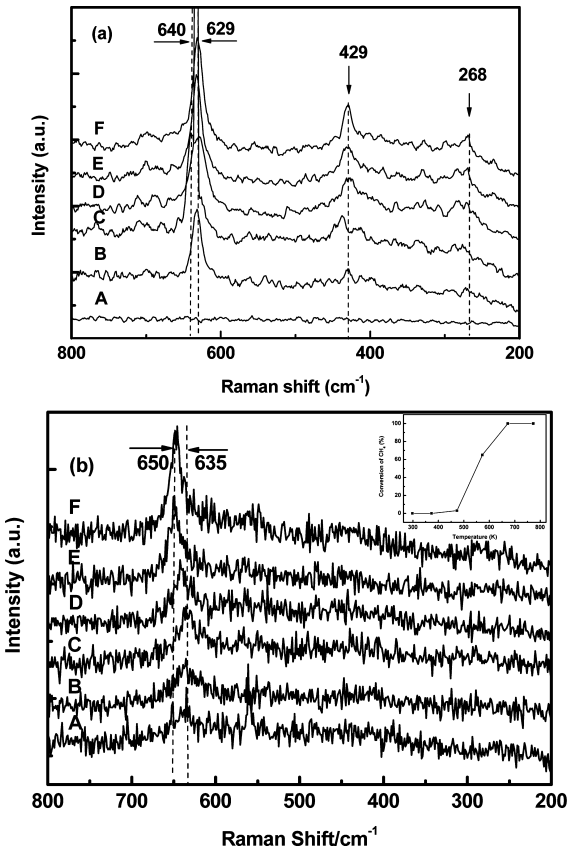

Figure 4. Temperature-dependent in situ Raman spectra (normalized) (a) in pure oxygen (3.0 kPa O_2, in He) and (b) in the mixture gas of methane + oxygen (0.5 kPa CH_4, 3.0 kPa O_2, in He). The temperature dependence on methane conversion is shown in the inset of the Figure 5b. Ramping rate, 10 °C/min; flow rate, 50 mL/min. Temp: (A) 298, (B) 373, (C) 473, (D) 573, (E) 673, and (F) 773 K.

peaks at 629, 429, and 268 cm^{-1} contributed by the Pd−O vibration in the PdO crystal could be determined up to 373 K. The one at 629 cm^{-1} is the strongest band that can be attributed to the B_{1g} mode; the relatively weaker and broader peaks at 429 and 268 cm^{-1} can be assigned to the E_g mode and the second order scattering,[36−38] respectively. The B_{1g} mode shifted from 629 cm^{-1} at 373 K to 640 cm^{-1} at 673 K, coupled with an increase in intensity. The changes in this vibration may be caused by the thermally induced growth of the PdO_x domain.

A similar tendency was also observed for other metal oxides, such as CeO_2 and Mn_3O_4.[39−43] Subsequently, the operando Raman spectra (Figure 4a) were recorded under the reaction conditions (0.5 kPa CH_4, 3.0 kPa O_2, rest He), and 100% conversion of methane was observed at 650 K (inset of Figure 4b). Furthermore, a small peak centered at 635 cm^{-1} at 298 K, which was also reported by Demoulin et al.[36] under similar conditions (1.0 kPa CH_4, 10.0 kPa O_2 and He on a 2 wt % Pd/γ-Al_2O_3 catalyst at 298 K), was found to grow with increasing temperature and then shifted to 650 cm^{-1} at 673 K. Moreover, the peaks corresponding to the E_g mode and the second-order scattering were too weak to be observed, indicating that the PdO_x species produced did not exist in the form of crystals, presumably, but were a layer-like PdO_x species. Valden et al.[44] reported that methane oxidation on the Pd(110) surface was controlled by competitive adsorption of methane and oxygen. It means the surface oxygen coverage during the reaction is lower than that in pure oxygen and, thus, reduces the rate for Pd oxidation.

The oxidation of metallic Pd during methane combustion has been studied for decades,[34,35] and the PdO_x species was proposed to play an important role in activating the methane molecule. In the model catalyst system, the initial temperature for Pd oxidation has been found to vary with different Pd crystal phases. For instance, Pd(111) could be oxidized at 723 K in 1.0 mPa O_2,[45] but this reaction occurred readily at 420 K for Pd(110).[46] However, it is still a debatable question. After they compared the kinetics of methane combustion from different Pd single crystals,[47] Zhu et al. argued that it is not a structure-sensitive reaction. Furthermore, Zhang and Altman[48] have proposed that Pd(111) oxidation proceeds through three stages involving four distinct surface states. The first stage is the chemisorption of atomic oxygen in a simple (2×2) layer in the temperature range 300−500 K; then, at or above 500 K, oxygen penetrates the surface, creating a rectangular structure that is further oxidized to bulk PdO_x. In particular, the formation of two intermediate Pd−O bonds from chemisorbed oxygen to bulk PdO_x has been confirmed. Of course, insights obtained from those model systems do not necessarily completely fit with real world catalyst systems. However, the kinetics of Pd → PdO_x in the model system is very valuable for the understanding of oxidation of polycrystalline Pd.

Actually, Ho et al.[49] found a similar oxidation process over a Pd/Al_2O_3 catalyst, in which oxygen could be first adsorbed on the Pd surface before penetrating into the Pd subsurface at or below ambient temperature, and bulk PdO_x was formed at ~800 K. Therefore, we assume that the oxidation of Pd in the present system should follow the same process. The PdO_x species detected by the operando Raman spectra (Figure 4b) may be derived from the second stage. Herein, a question arises logically of how many metallic Pd atoms were oxidized during reaction. To answer this intricate question, for the first time, efforts have been made by using in situ DRIFTS spectra using CO as the probe molecule.

The spectra in Figure 5a were recorded at 298 K after reaction at different temperatures. Four distinct peaks were

dx.doi.org/10.1021/cs200694k | ACS Catal. 2012, 2, 261−269

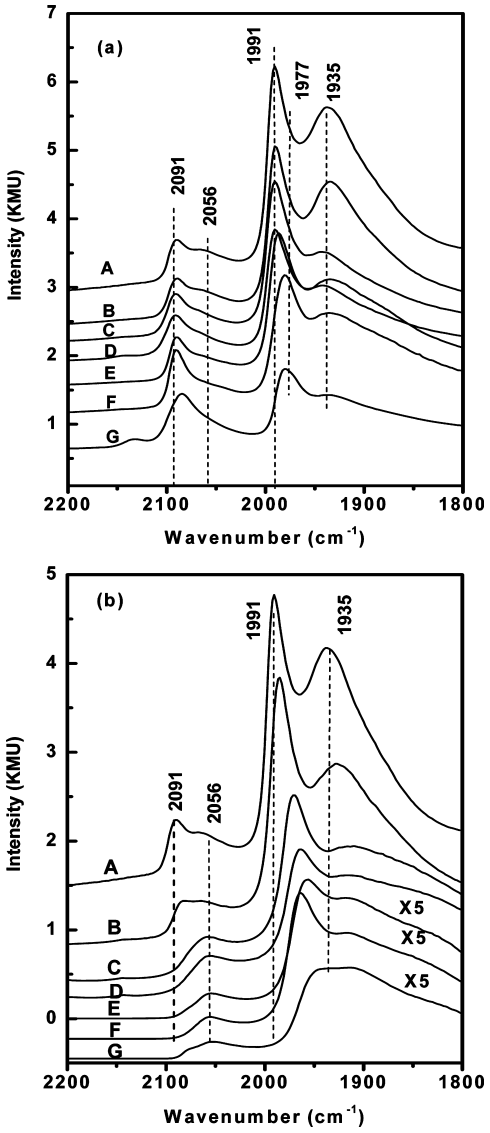

Figure 5. In situ DRIFTS of CO adsorption over the reacted catalyst surfaces (a) recorded at 298 K after reaction at different temperatures: (A) 298, (B) 373, (C) 473, (D) 573, (E) 623, (F) 673, and (G) 773 K and (b) recorded at reaction temperatures (A) 298, (B) 373, (C) 473, (D) 573, (E) 623, (F) 673, and (G) 773 K. The reaction was carried out in a stream of 0.5 kPa CH_4, 3.0 kPa O_2 in He at a flow rate of 20 mL/min for 2 h.

assigned in accordance with previous studies listed in Table 4. The bands at 2091 cm^{-1} resulted from the stretching vibrations of the linear adsorbed CO bonds (Pd−CO) at Pd atoms of low coordination, at corner or edge positions of particles. The asymmetric shape of this band, tailing toward 2056 cm^{-1}, indicated the presence of a quite heterogeneous population of Pd metal sites. The bands at 1991 and 1935 cm^{-1} can be attributed to the bridge Pd_2−(CO) bonds in the compressed and isolated states, respectively. In addition, the band at 1935 cm^{-1} may also be caused by a bridge Pd_3^+−(CO) bond. With an increase in temperature to 673 K, the peaks shifted down by Δ7 cm^{-1} while the intensities for the bridged species declined significantly. A small peak at 2143 cm^{-1} corresponding to oxide Pd was observed.

Figure 5a also indicates the coexistence of both metallic and oxide Pd on the spent catalyst surfaces. However, it may not fully reflect the real "working state" of the catalyst, since the reconstruction of the Pd surface may occur during the cooling process. For this reason, the spectra illustrated in Figure 5b were recorded immediately for the reacted catalysts while sacrificing signal intensity. Those bands remained from 298 to 373 K; however, the band at 2091 cm^{-1} disappeared completely at 398 K, whereas the band at 2056 cm^{-1} could be observed until 673 K. Meanwhile, the bridge band at 1991 cm^{-1} shifted to 1954 cm^{-1}, but the band at 1935 cm^{-1} almost faded away. More interestingly, when zooming in the region of 2050−2200 cm^{-1} (Figure 5b), a weak peak centered at 2141 cm^{-1} was seen at 473 K and shifted to 2132 cm^{-1} at 673 K, accompanied by rapid growth in its intensity (Figure 6). In line with previous studies,[48−52] this band may correspond to a linear CO−Pd^{2+} bond, an indication of the existence of PdO_x species.

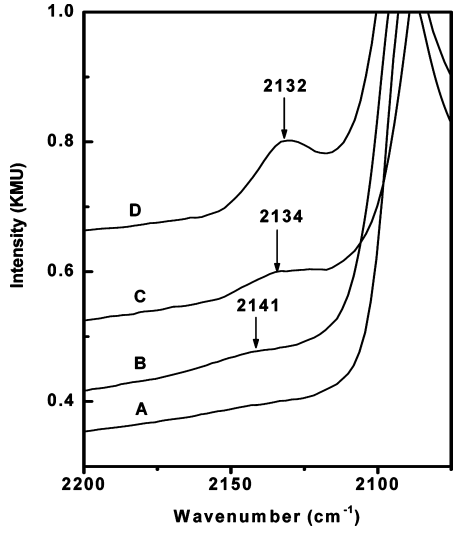

Figure 6. In situ DRIFTS of CO adsorption in the region of 2050−2200 cm^{-1} derived from Figure 5a. (A) 298, (B) 473, (C) 573, and (D) 673 K.

Table 4. IR Bands of CO Absorbed Unsupported and Supported Pd/Al_2O_3

ν (cm^{-1})	species	refs
2160−2145	Pd^{2+}−CO (linear)	50−52
2135−2110	Pd^{+}−CO (linear)	19, 50−53, this study
2000−2050	Pd^{0}−CO (linear)	50−54, this study
2000−1960	Pd_2(CO) compressed, CO/Pd (100) faces, or Pd_2^+(CO) (bridged)	56−60, this study
1950−1900	Pd_2(CO) isolated, CO/Pd(111) faces, or Pd_3^+(CO) (bridged)	56−60, this study

DRIFTS of CO adsorption have demonstrated that the features of the Pd working surfaces are quite different from that recorded from the postreaction catalysts. Combining XPS, LRS, and DRIFTS spectra, we infer that only part of the surface Pd atoms can be oxidized into PdO_x under the current reaction conditions. This assertion is consistent with the observations from Baiker's group.[55] Furthermore, the number of Pd atoms oxidized at different temperatures was roughly evaluated on the basis of the DRIFTS results.

dx.doi.org/10.1021/cs200694k | ACS Catal. 2012, 2, 261−269

From Figure 5a, all bands in the region of 2100−1800 cm^{-1} can be assumed to result from CO adsorption on the metallic Pd atoms, and their intensities in Kubelka−Munk are dependent on the amount of adsorbed CO[61] that is proportional to the number of Pd active sites. Given that the total intensity (peak height) for all peaks at 298 K (spectrum A in Figure 5a) represents all metallic Pd atoms in the surface layer, a decrease in the peak intensity will be inversely proportional to the number of oxidized Pd atoms (see the caption of Figure 7).

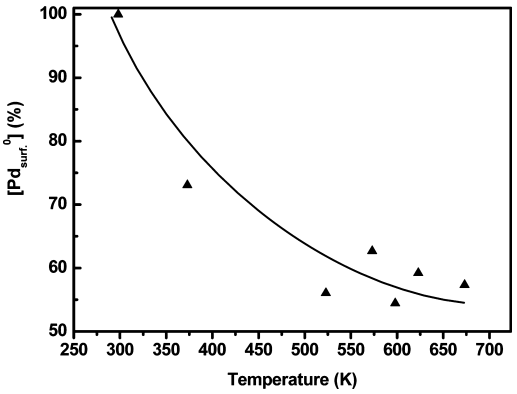

Figure 7. The concentration of the metallic Pd atom (Pd^0_{surf}) on the catalyst surface as a function of the reaction temperature. The data were calculated on the basis of the spectra in Figure 6: $Pd^0_{surf}(\%) = I_T/I_{298} \times 100\%$, where I is the total intensity of all bands (peak height for linear and bridged CO-Pd bonds) and the subscript T is the reaction temperature.

The rate for Pd oxidation decreased with an increase in the temperature (Figure 7). About 25% of the surface Pd atoms were converted at 373 K and 45% at 523 K, and nearly half of the metallic Pd atoms remained unchanged until 673 K. It is worth noting that the potential reduction of PdO_x to metallic Pd due to CO adsorption can be ruled out because no linear CO−Pd bond was observed by introducing CO to a PdO_x/γ-Al_2O_3 catalyst at 298 K, which was produced by treating the Pd/γ-Al_2O_3 catalyst in pure O_2 at 673 K for 30 min, followed by cooling to 298 K in He.

3.3. Plausible Mechanism. The mechanism for catalytic oxidation/combustion of methane over Pd catalysts has long been debated.[9] Generally, those reactions were proposed to proceed through two pathways: (i) the Langmuir−Hinshelwood mechanism, in which adsorbates interacted on the catalyst surface, and (ii) the Mars−van-Krevelen mechanism, in which methane molecules or its dissociative species were oxidized by the lattice oxygen. In particular, the latter is supposed to be dominant at elevated temperatures (>773 K) (see ref 9 and references therein). To distinguish this study from previous works, the following discussion is limited to the reaction behaviors below 673 K.

The positive reaction orders with respect to both methane and oxygen (Figure 1) indicate that methane combustion proceeds primarily through the Langmuir−Hinshelwood mechanism, by which the adsorbed methane and its intermediates (CH_χ and C, $\chi \leq 3$) react with the adsorbed oxygen on the metallic Pd surface. Dissociative adsorption of methane has been studied on various single crystal Pd's, such as Pd(111), Pd(311), and Pd(679).[44,62,63] The adsorption of methane could take place at 400 K, and the initial rate for methane dissociation varied with the property of the surfaces. For instance, the rate of methane dissociation on Pd(679) is larger than that on Pd(111) by 1 order of magnitude because of more steps and kinks in the Pd(679) surface. Pd atoms in the polycrystalline form have more uncoordinated sites than that for the single crystal surfaces; it leads to a relatively high rate. In addition, because of competitive adsorption of methane and oxygen,[44] the reaction rate for the oxygen-precovered Pd surface should be lower than that for the fresh reduced catalyst. As listed in Table 1, the reaction orders with respect to methane at or below 773 K approach 1 for different Pd/γ-Al_2O_3 catalysts, indicating that the dissociative adsorption of methane may be a rate-limiting step.[64,65]

The spectra in Figures 3−6 suggested that the adsorption of oxygen and Pd oxidation could occur simultaneously during reaction, and about half of metallic Pd remained unchanged, even at 673 K, according to the DRIFTS spectra (Figure 7). We argue that under the current reaction conditions, activating methane should mainly take place on the metallic Pd sites. Thus, most of the active oxygen did not likely originate from the lattice oxygen of PdO_x, as previously suggested, but rather, from adsorbed oxygen. More interestingly, Ciuparu et al. reported that the active oxygen might come from supporters through spillover when the reaction was carried out in pulses of the reaction mixture labeled with $^{18}O_2$ over the Pd/Al_2O_3 and Pd/ZrO_2 catalysts.[66]

In this study, the reaction order with respect to oxygen decreased from 0.86 at 473 K to 0.16 at 673 K (Table 3), and the strong dependency of the reaction rates on the p_{O_2} at 473 K indicate that the oxygen coverage on the Pd surface was unsaturated, probably because of competitive adsorption of oxygen and methane that suppressed oxygen adsorption. The remarkable decrease in the reaction order with respect to oxygen at 673 K indicates that except for the adsorbed oxygen, the lattice oxygen from PdO_x species may be increasingly involved in activating methane and the subsequent reaction; that is to say, methane is probably oxidized simultaneously through the Mars−van-Krevelen mechanism with an increase in the temperature.

Clearly, by in situ/operando spectroscopy, we are able to envisage a structural profile of the working Pd catalyst during low-temperature methane combustion. The combination of kinetics and spectroscopy allows us to explain the reaction behaviors by plausible mechanisms. This study also reminds us that there is much room for improving the performance of Pd-based catalysts for methane lean-burn combustion at low temperatures if the metallic Pd sites can be stabilized during reaction; for instance, through alloying with other metals.

4. CONCLUSIONS

In this work, the following conclusions can be drawn:

(1) During methane combustion, operando Raman spectra have demonstrated that the oxidation of Pd could occur as low as room temperature during methane combustion; the oxidation rate for Pd → PdO_x was found to decrease with rising temperature. Nearly 50% of the metallic Pd atoms on the surface were oxidized to PdO_x at 673 K, as evidenced by in situ DRIFTS spectra.

(2) In accordance with the kinetic features, especially the variation of the reaction order with respect to oxygen (from 0.86 at 473 K to 0.16 at 673 K), methane combustion occurs mainly on the metallic Pd sites at 473 K, whereas PdO_x species may involve the reaction increasingly with an increase in the temperature to 673 K.

dx.doi.org/10.1021/cs200694k | ACS Catal. 2012, 2, 261−269

Those results suggest that the stability of metallic state Pd is very important for keeping its reactivity toward methane combustion at low temperatures.

AUTHOR INFORMATION

Corresponding Author

*Phone: +86-21-64251928. Fax: +86-21-64251928. E-mail: yifanhan@ecust.edu.cn.

ACKNOWLEDGMENTS

The authors are grateful for support from the Chinese Education Ministry 111 project (B08021), the National Natural Science Foundation of China (21176071, 21106041, 20973113), the Shanghai PuJiang Talent Program (2010/10PJ1402500, 2011/11PJ1402400), the Innovation Program of the Shanghai Municipal Education Commission (11ZZ52, 11ZZ051), the Shanghai Natural Science Foundation (11ZR1408400), the Opening Project Program of the State Key Laboratory of Chemical Engineering (SKL-ChE-10C05), the program of the Science and Technology Commission of the Shanghai Municipality (11JC1402700), the Creative Team Development Project of the Ministry of Education (IRT0721), and the Fundamental Research Funds for the Central Universities.

REFERENCES

(1) Zarur, A. J.; Ying, J. Y. *Nature* **2000**, *403*, 65−67.
(2) Zwinkels, M. F. M.; Järås, S. G.; Menon, P. G.; Griffin, T. A. *Catal. Rev. Sci. Eng.* **1993**, *35*, 319−358.
(3) Charlson, R. J. *Nature* **2005**, *438*, 165−166.
(4) Han, Y.-F.; Chen, L. W.; Ramesh, K.; Widjaja, E.; Chilukoti, S.; Surjami, I. K.; Chen, J. *J. Catal.* **2008**, *253*, 261−268.
(5) Han, Y.-F.; Chen, F.; Zhong, Z. Y.; Ramesh, K.; Chen, L. W.; Widjaja, E. *J. Phys. Chem. B* **2006**, *110*, 24450−24456.
(6) Marín, P.; Hevia, M. A. G.; Ordóñez, S.; Díez, F. V. *Catal. Today* **2005**, *105*, 701−708.
(7) Yao, Y. F. Y. *Ind. Eng. Chem. Prod. Res. Dev.* **1980**, *19*, 293−298.
(8) Yang, L.; Shi, C.; He, X.; Cai, J. *Appl. Catal., B* **2002**, *38*, 117−125.
(9) Ciuparu, D.; Lyubovsky, M. R.; Altman, E.; Pfefferle, L. D.; Datye, A. *Catal. Rev.* **2002**, *44*, 593−649.
(10) Gélin, P.; Primet, M. *Appl. Catal., B* **2002**, *39*, 1−37.
(11) Castellazzi, P.; Groppi, G.; Forzatti, P.; Finocchio, E.; Busca, G. *J. Catal.* **2010**, *275*, 218−227.
(12) Mallika, C.; Sreedharan, O. M.; Gnanamoorthy, J. B. *J. Less-Common Met.* **1983**, *95*, 213−220.
(13) Burch, R.; Urbano, F. J. *Appl. Catal., A* **1995**, *124*, 121−138.
(14) Müller, C. A.; Maciejewski, M.; Koeppel, R. A.; Tschan, R.; Baiker, A. *J. Phys. Chem.* **1996**, *100*, 20006−20014.
(15) Fujimoto, K.-I.; Ribeiro, F. H.; Avalos-Borja, M.; Iglesia, E. *J. Catal.* **1998**, *179*, 431−442.
(16) Ciuparu, D.; Altman, E.; Pfefferle, L. *J. Catal.* **2001**, *203*, 64−74.
(17) Au-Yeung, J.; Chen, K.; Bell, A. T.; Iglesia, E. *J. Catal.* **1999**, *188*, 132−139.
(18) Kanezaki, E.; Takana, S.; Murai, K.-I.; Moriga, T.; Motonaka, J.; Katoh, M.; Nakabayashi, I. *Anal. Sci.* **2004**, *20*, 1069−1073.
(19) Demoulin, O.; Navez, M.; Ruiz, P. *Appl. Catal., A* **2005**, *295*, 59−70.
(20) Lee, J. H.; Trimm, D. L. *Fuel Process. Technol.* **1995**, *42*, 339−359.
(21) Cullis, C. F.; Keene, D. E.; Trimm, D. L. *Trans. Faraday Soc.* **1971**, *67*, 864−876.
(22) Demoulin, O.; Navez, M.; Ruiz, P. *Catal. Today* **2006**, *112*, 153−156.
(23) Ribeiro, F. H.; Chow, M.; Dalla Betta, R. A. *J. Catal.* **1994**, *146*, 537−544.
(24) Julien, C. M.; Massot, M.; Poinsignon, C. *Spectrochim. Acta, Part A* **2004**, *60*, 689−700.
(25) Le Bourdon, G.; Adar, F.; Moreau, M.; Morel, S.; Reffner, J.; Mamede, A. S.; Dujardin, C.; Payen, E. *Phys. Chem. Chem. Phys.* **2003**, *5*, 4441−4444.
(26) Tinnemans, S. J.; Mesu, J. G.; Kervinen, K.; Visser, T.; Nijhuis, T. A.; Beale, A. M.; Keller, D. E.; van der Eerden, A. M. J.; Weckhuysen, B. M. *Catal. Today* **2006**, *113*, 3−15.
(27) Zhang, J.; Li, M.; Feng, Z.; Chen, J.; Li, C. *J. Phys. Chem. B* **2006**, *110*, 927−935.
(28) Li, M.; Feng, Z.; Ying, P.; Xin, Q.; Li, C. *Phys. Chem. Chem. Phys.* **2003**, *5*, 5326−5332.
(29) Li, C.; Li, M. *J. Raman Spectrosc.* **2002**, *33*, 301−308.
(30) Banares, M. A. *Catal. Today* **2005**, *100*, 71−77.
(31) Matam, S. K.; Aguirre, M. H.; Weidenkaff, A.; Ferri, D. *J. Phys. Chem. C* **2010**, *114*, 9439−9443.
(32) Koros, R. M.; Nowak, E. J. *Chem. Eng. Sci.* **1967**, *22*, 470−475.
(33) Cullis, C. F.; Willatt, B. M. *J. Catal.* **1983**, *83*, 267−285.
(34) Voogt, E. H.; Mens, A. J. M.; Gijzeman, O. L. J.; Gens, J. W. *Surf. Sci.* **1996**, *350*, 21−31.
(35) Zhu, G.; Han, J.; Zemlyanov, D. Y.; Ribeiro, F. H. *J. Phys. Chem. B* **2005**, *109*, 2331−2337.
(36) Demoulin, O.; Navez, M.; Gaigneaux, E. M.; Ruiz, P.; Mamede, A.-S.; Granger, P.; Payen, E. *Phys. Chem. Chem. Phys.* **2003**, *5*, 4394−4401.
(37) Otto, K.; Hubbard, C. P.; Weber, W. H.; Graham, G. W. *Appl. Catal., B* **1992**, *1*, 317−327.
(38) Weber, W. H.; Baird, R. J.; Graham, G. W. *J. Raman Spectrosc.* **1988**, *19*, 239−244.
(39) Graham, G. W.; Weber, W. H.; Peters, C. R.; Usmen, R. *J. Catal.* **1991**, *130*, 310−313.
(40) Patil, S.; Seal, S.; Guo, Y.; Schulte, A.; Norwood, J. *Appl. Phys. Lett.* **2006**, *88*, 243110−243116.
(41) Weber, W. H.; Hass, K. C.; McBride, J. R. *Phys. Rev. B* **1993**, *48*, 178−185.
(42) Rodriguez, J. A.; Wang, X.; Hanson, J. C.; Liu, G.; Iglesias-Juez, A.; Fernández-García, M. *J. Chem. Phys.* **2003**, *119*, 5659−5669.
(43) Zuo, J.; Xu, C.; Liu, Y.; Qian, Y. *Nanostruct. Mater.* **1998**, *10*, 1331−1335.
(44) Valden, M.; Pere, J.; Hirsimäki, M.; Suhonen, S.; Pessa, M. *Surf. Sci.* **1997**, *605*, 377−379.
(45) Légaré, P.; Hilaire, L.; Maire, G. *Surf. Sci.* **1981**, *107*, 533−546.
(46) Milum, M.; Pervan, P.; Vajić, M.; Wandelt, K. *Vacuum* **1990**, *40*, 105−107.
(47) Zhu, G.; Han, J.; Zemlyanov, D. Y.; Ribeiro, F. H. *J. Am. Chem. Soc.* **2004**, *126*, 9896−9897.
(48) Zheng, G.; Altman, E. I. *Surf. Sci.* **2000**, *462*, 151−168.
(49) Ho, Y.-S.; Wang, C.-B.; Yeh, C.-T. *J. Mol. Catal. A: Chem.* **1996**, *112*, 287−294.
(50) Tessier, D.; Rakai, A.; Bozon-Verduraz, F. *J. Chem. Soc. Faraday Trans.* **1992**, *88*, 741−749.
(51) Amalric-Popescu, D.; Bozon-Verduraz, F. *Catal. Lett.* **2000**, *64*, 125−128.
(52) Skotak, M.; Karpiński, Z.; Juszczyk, W.; Pielaszek, J.; Kępiński, L.; Kazachkin, D. V.; Kovalchuk, V. I.; d'Itri, J. L. *J. Catal.* **2004**, *227*, 11−25.
(53) Juszczyk, W.; Karpiński, Z.; Ratajczykowa, I.; Stanasiuk, Z.; Zieliński, J.; Sheu, L.-L.; Sachtler, W. M. H. *J. Catal.* **1989**, *120*, 68−77.
(54) Benkhaled, M.; Morin, S.; Pichon, Ch.; Tomazeau, C.; Verdon, C.; Uzio, D. *Appl. Catal., A* **2006**, *312*, 1−11.
(55) van Vegten, N.; Marek, M.; Krumeich, F.; Baiker, A. *Appl. Catal., B* **2009**, *93*, 38−49.
(56) Wei, T.; Wang, J.; Goodman, D. W. *J. Phys. Chem. C* **2007**, *111*, 8781−8788.
(57) Ortega, A.; Hoffman, F. M.; Bradshaw, A. M. *Surf. Sci.* **1982**, *119*, 79−94.
(58) Bradshaw, A. M.; Hoffmann, F. M. *Surf. Sci.* **1975**, *52*, 449−454.
(59) Bradshaw, A. M.; Hoffmann, F. M. *Surf. Sci.* **1978**, *72*, 513−535.

(60) Garbowski, E.; Feumi-Jantou, C.; Mouaddib, N.; Primet, M. *Appl. Catal., A* **1994**, *109*, 277−291.
(61) Yang, S.; Maroto-Valiente, A.; Benito-Gonzalez, M.; Rodriguez-Ramos, I.; Guerrero-Ruiz, A. *Appl. Catal., B* **2000**, *28*, 223−233.
(62) Kubelka, P.; Munk, F. *Z. Tekn. Phys.* **1931**, *12*, 593−601.
(63) Wang, Y.-N.; Herman, R. G.; Klier, K. *Surf. Sci.* **1992**, *279*, 33−48.
(64) Klier, K.; Hess, J. S.; Herman, R. G. *J. Chem. Phys.* **1997**, *107*, 4033−4043.
(65) Maillet, T.; Solleau, C.; Barbier, J.; Duprez, D. Jr. *Appl. Catal., B* **1997**, *14*, 85−95.
(66) Ciuparu, D.; Bozon-Verduraz, F.; Pfefferle, L. *J. Phys. Chem. B* **2002**, *106*, 3434−3442.